Chinese Chemical Letters 33 (2022) 3941–3946

Contents lists available at ScienceDirect

Chinese Chemical Letters

journal homepage: www.elsevier.com/locate/cclet

HSH-C_{10}: A new *quasi*-2D carbon allotrope with a honeycomb-star-honeycomb lattice

Qian Gao[a], Lifu Zhang[a], Caiyan Zheng[a], Shulai Lei[b,*], Shujuan Li[b,c], Zhenpeng Hu[a,*]

[a] School of Physics, Nankai University, Tianjin 300071, China
[b] Hubei Key Laboratory of Low Dimensional Optoelectronic Materials and Devices, Hubei University of Arts and Science, Xiangyang 441053, China
[c] Institute of Mathematics, Free University of Berlin, Arnimallee 6, Berlin D-14195, Germany

ARTICLE INFO

Article history:
Received 18 August 2021
Revised 12 October 2021
Accepted 4 November 2021
Available online 11 November 2021

Keywords:
Carbon allotrope
Two-dimensional lattice
Charge-shift bond
Flat band
First-principles

ABSTRACT

Two-dimensional (2D) materials with honeycomb, kagome or star lattice have been intensively studied because electrons in such lattices could give rise to exotic quantum effects. In order to improve structural diversity of 2D materials to achieve unique properties, here we propose a new *quasi-2D* honeycomb-star-honeycomb (HSH) lattice based on first-principles calculations. A carbon allotrope named HSH-C_{10} is designed with the HSH lattice, and its mechanical properties have been intensively investigated through total energy, phonon dispersion, ab initio molecular dynamic simulations, as well as elastic constants calculations. Besides the classical covalent bonds, there is an interesting charge-shift bond in this material from the chemical bonding analysis. Additionally, through the analysis of electronic structure, HSH-C_{10} is predicted to be a semiconductor with a direct band gap of 2.89 eV, which could combine the desirable characteristics of honeycomb and star lattice. Importantly, by modulating coupling strength, a flat band near the Fermi level can be obtained in compounds HSH-C_6Si_4 and HSH-C_6Ge_4, which have potential applications in superconductivity. Insight into such mixed lattice would inspire new materials with properties we have yet to imagine.

The unique two-dimensional (2D) lattices, like honeycomb lattice [1], kagome lattice [2] and star lattice [3], have been intensively studied because electrons in such lattices could give rise to exotic quantum effects. The honeycomb lattice could induce Dirac bands, while the kagome lattice and star lattice could induce both Dirac bands and flat bands [1–5]. They are interesting subjects to study various properties in quantum fields, such as quantum spin liquid, frustrated spin, and fractional quantum Hall effect [6]. Especially, the kinetic energy of electrons is quenched in the flat bands, which is helpful to realize strongly correlated electronic states, such as superconductivity and Wigner crystal [7,8]. These lattices not only provide ideal research platforms for understanding novel physics, but also have potential applications in electronics and spintronics [9–14].

Many studies have focused on the practical application of materials with unique lattices based on the special properties [15–22] mentioned above. With honeycomb lattice, graphene is one of the most widely investigated 2D carbon allotropes [23]. It has also actively encouraged and promoted the research on other 2D topological materials with honeycomb lattice, like silicene, germanene, and stanine [24–26]. Besides structures with honeycomb lattice, various structures with kagome lattice have also been proposed [27–29]. Materials with kagome lattice usually exhibit interesting properties. For example, it is reported that the designed phosphorus carbide P_2C_3 with kagome lattice contains double kagome bands, which is named from the property that the flat band in one kagome band accidently crossing the Dirac point in the other kagome band [30]. And the experimental evidence of flat band in a kagome lattice has been observed in twisted bilayer silicene, making it a possible candidate for realizing exotic quantum Hall states [31]. Recently, a star carbon monolayer was also proposed with a flat band near the fermi level [32,33]. By the tight-binding models on the decorated star lattices, Mizoguchi and his co-authors proposed a class of carbon-based materials with exotic electronic structures such as Dirac cones and flat bands [34].

To design novel 2D materials, a new route which mixes different lattices in structures has been devised recently. A novel honeycomb–kagome (HK) lattice was proposed, which could be regarded as a mixed lattice composed of honeycomb and kagome lattices [35–39]. Comparing the single lattice, the mixed lattice signif-

* Corresponding authors.
E-mail addresses: sllei@hbuas.edu.cn (S. Lei), zphu@nankai.edu.cn (Z. Hu).

https://doi.org/10.1016/j.cclet.2021.11.027
1001-8417/

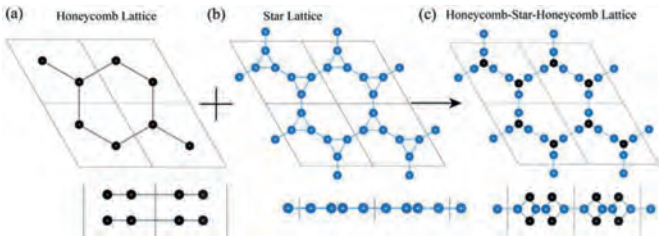

Fig. 1. The top and side views of (a) bilayer honeycomb lattice, (b) star lattice, and (c) honeycomb-star-honeycomb lattice.

icantly increases the structural diversity of 2D materials and could provide more opportunities to achieve unique properties [40]. With experimental synthesis methods making rapid progress, practical methods are being explored to establish well-defined manufacturing techniques to realize the mixed lattices. For example, a spin-superstructure with honeycomb-triangular lattice was realized experimentally, which the magnetic layers in triangular and honeycomb lattices exhibit sequential magnetic orderings [41]. It is noted that the novel 2D materials with a mixed lattice have quickly attracted significant attention and would be a potential research focus.

In this study, a new *quasi*-2D honeycomb-star-honeycomb (HSH) lattice was proposed. The idea of the lattice was sprung up by the peculiar features of honeycomb lattice and star lattice. Material with such a mixed lattice would combine the desirable characteristics of both honeycomb and star lattices. The carbon-based materials would induce various characteristic electronic structures, and thus become our primary consideration to probe the physical and chemical properties. The dynamical, thermal and mechanical stability as well as the electronic properties are evaluated. It is expected that more new materials with exotic properties could be designed based on this mixed lattice.

In this study, all the studies were conducted based on density functional theory (DFT), as implemented in the Vienna ab initio simulation package (VASP) [42,43]. The Perdew–Burke–Ernzerhof (PBE) [44] exchange-correlation functional and PAW [45] pseudopotential were used. The electronic wave function was expanded in plane waves to a cut-off energy of 520 eV. For the unit cell and the $p(2 \times 2 \times 1)$ supercell, Monkhorst-Pack meshes with $6 \times 6 \times 1$ and $3 \times 3 \times 1$ in Brillouin zone sampling were used, respectively. To avoid interactions between the repeated images, the vacuum thickness larger than 16 Å was used. All the structures were relaxed with no symmetry constraint, and the convergence criteria for total energy and residual force on each ion were set to 10^{-5} eV and 0.01 eV/Å, rescpectively. The phonon calculations were performed using PHONOPY package [46] with the forces calculated from density functional perturbation theory (DFPT) [47] as implemented in VASP. Because the convergence of phonon frequencies needs higher energy accuracy than normal electronic structure calculations, the total energy was converged to less than 10^{-8} eV in all the phonon calculations.

The star lattice can be considered as an expanded honeycomb lattice which replacing the sites of the honeycomb lattice by triangles. The HSH lattice is a mixed lattice with a star lattice sandwiched by two honeycomb lattices, as shown in Fig. 1. Such lattice would significantly increase the structural diversity of 2D materials and provide more opportunities to achieve unique properties. Carbon is not only containing various allotropes, but also has the richest variety of compounds among all elements. As a preliminary exploration of the application in real materials, we designed a carbon allotrope based on the HSH lattice. The honeycomb lattice containing four atoms and the star lattice containing six atoms, the new carbon allotrope is named HSH-C_{10}.

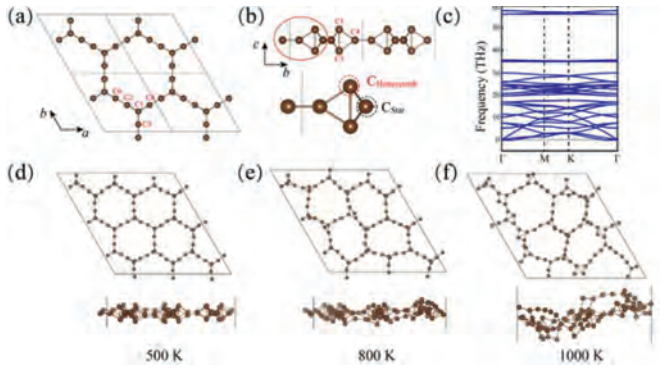

Fig. 2. (a) The top and (b) side views of HSH-C_{10}, (c) the phonon dispersion along high symmetry directions of Brillouin zone, and (d–f) final structures with ab initio molecular dynamic simulations under the temperature of 500, 800 and 1000 K.

The top and side views of HSH-C_{10} are illustrated in Figs. 2a and b. From a linear scan on the lattice constant (Fig. S1 in Supporting information), the carbon allotrope has a hexagonal cell with a lattice constant of 6.60 Å and two different carbons with three different bond lengths. Six carbon atoms are marked from C1 to C6, as shown in Fig. 2a and b. The lengths of three bonds marked as C2-C6, C1-C2, and C1-C3 are 1.30, 1.51 and 1.67 Å, respectively. The carbon atom in honeycomb lattice is named $C_{Honeycomb}$ (C1, C3), while the one in star lattice is named C_{Star} (C2, C4, C5, C6). For comparison, the energy of all the systems is defined as DFT computed ground-state energy per atom. The energies of graphene [48], two carbon allotropes (named as C-phase 1 and 2 here) [49], E-graphene [50], as well as graphdiyne [51] are also calculated, and details of all the structures are shown in Table 1. Graphene is the most energetically stable allotrope, and the energy of −9.22 eV/atom is the same as previous DFT simulations [52]. The energy of HSH-C_{10} is −7.80 eV/atom, which is higher than graphene and graphdiyne (−8.46 eV/atom), but lower than C-phase 1 (−7.45 eV/atom), and a little higher than C-phase 2 (−7.93 eV/atom) and E-graphene (−7.93 eV/atom). The bond lengths of 1.51 and 1.67 Å in HSH-C_{10} are a little higher than the two kinds of bond lengths for C-phase 2 (1.50 and 1.59 Å), while the bond length of 1.30 Å is much smaller than that in C-phase 2. Furthermore, the recently reported T-carbon has an energy of −7.92 eV/atom [53], which is closed to the energy of C-phase 2. Obviously, the relative energy of HSH-C_{10} structure is lower than C-phase 1 and much close to C-phase 2 and T-carbon. Since C-phase 1 is predicted to be stable at a low temperature [49] and T-carbon is already realized in the experiments [54], it is believed there would be a high possibility to realize the HSH-C_{10} structure experimentally based on the energy data.

From a structural analysis, the relatively high energy of this material comes from the formed hexahedral structure. The four bonds of $C_{Honeycomb}$ atom point to the same side, leading to the inverted bond $C_{Honeycomb}$-$C_{Honeycomb}$ (C1-C3) embedded inside a cage of six wing $C_{Honeycomb}$-C_{Star} bonds, thus generating relatively high strain energy. Interestingly, the hexahedral structure is the same as [1.1.1]propellane, which is a hydrocarbon with the molecular formula C_5H_6 and could be synthesized in large quantities [55,56]. It is reported that this molecule has remarkable stability despite the supposed strain energy from the inverted bridgehead bond [57–61]. For comparison, the structure of [1.1.1]propellane is also shown in Fig. S2 (Supporting information). As listed in Table 1, the PBE calculated inverted bond length for [1.1.1]propellane is 1.58 Å, consistent with the experimental results of 1.59 Å [62], and little shorter than the $C_{Honeycomb}$-$C_{Honeycomb}$ bond length of 1.67 Å in HSH-C_{10}. As reported [61], the inverted bond is a charge-shift bond, which is regarded as a third kind of chemical

Table 1
The number of carbon atoms in unit cell (N), lattice constants (a and b), total energy per atom (E_{tot}) and bond length ($d_{C\text{-}C}$) for HSH-C_{10}. For comparison, the corresponding parameters for graphene, two carbon allotropes (named as C-phase1 and 2), E-graphene, graphdiyne, and [1.1.1]propellane molecule are also provided here.

Structure	N	a/b (Å)	E_{tot} (eV/atom)	$d_{C\text{-}C}$ (Å)
HSH-C_{10}	10	6.60/6.60	−7.80	1.30, 1.51, 1.67
graphene [48]	2	2.46/2.46	−9.22	1.42
C-phase 1 [49]	2	2.47/1.65	−7.45	1.51, 1.65
C-phase 2 [49]	8	2.50/7.01	−7.93	1.50, 1,59
E-graphene [50]	8	2.50/6.58	−7.93	1.50, 1.60
graphdiyne [51]	18	9.46/9.46	−8.46	1.43, 1.40, 1.23, 1.34
[1.1.1]propellane [62]	5	/	/	1.52, 1.58

bond in addition to the ionic and covalent bonds. The charge-shift bond shows large covalent-ionic resonance interaction energy and depleted charge densities, but the bond itself could well be strong [57–61]. From the structural connection, it is promising that HSH-C_{10} could be synthesized by the polymerization of [1.1.1]propellane.

To further confirm the dynamical stability of HSH-C_{10} structure, the calculations of phonon dispersion are also performed. A $p(2 \times 2 \times 1)$ supercell is used to calculate the vibrational modes of HSH-C_{10} along the high symmetry k-points throughout the first Brillouin zone. As shown in Fig. 2c, the phonon dispersion of HSH-C_{10} has little imaginary frequency less than 4 cm^{-1} close to Γ point. As the little imaginary frequency in long wavelength flexural acoustic (ZA) mode close to Γ point is the feature of *quasi*-2D materials [63–66], the phonon dispersion indicates HSH-C_{10} is dynamically stable. Besides, the highest frequency of HSH-C_{10} reaches up to 58 THz (1935 cm^{-1}), a little higher than that of graphene (1600 cm^{-1}) [67], confirming the robust C–C bonding in 2D HSH-C_{10} sheet. There also exists a large direct bandgap of 20 THz (~667 cm^{-1}) at the Γ point in the phonon band structures, which would be useful to identify the structure of HSH-C_{10} in experiments.

Ab initio molecular dynamic simulations in a Nose-Hoover thermostat are also performed to check the thermal stability. A $p(3 \times 3 \times 1)$ supercell containing 90 carbon atoms is built to reduce the constraint of periodic boundary condition and explore the possible structure reconstruction. Molecular dynamic simulations under the temperature of 500, 800, 1000 K for 10 ps are performed, and the final structures are depicted in Figs. 2d–f. With no bonds breaking in the whole simulation, the structure is stable under the temperature of 500 K. Under the temperature of 800 K, the charge-shift bond (C1-C3) would fluctuate relatively greatly. When the temperature is heated to 1000 K, obvious structure reconstruction is found. The molecular dynamic simulations suggest that HSH-C_{10} is separated by high energy barriers from other local minima on the potential energy surface.

The mechanical properties of HSH-C_{10} are also studied in this work. The elastic constants of materials based on theoretical calculations are not only important for the potential applications, but also could be used to investigate the mechanical stabilities. The finite distortion method is used to calculate the linear elastic constants [68]. The independent elastic constants C_{ij} can be then expressed as $C_{ij} = \partial F/\partial\varepsilon_i\varepsilon_j$, and the strain energy density function F is expressed as $F = F_0 + F^2\varepsilon^2/2 + O(\varepsilon^3)$, where F_0 and $F^2\varepsilon^2/2$ are the static energy and the vibrational contribution, respectively.There are three independent elastic constants for the hexagonal structure, which are C_{11} (C_{22}=C_{11}), C_{12} and C_{44}. Based on Born-Huang criteria [69], the mechanical stability for a 2D material needs to satisfy C_{11}>C_{12} and C_{44}>0. By fitting the strain energy to the parabolic function of the axial and biaxial strains, it is obtained that $C_{22} = C_{11} = 394.14$ N/m, $C_{12} = 384.42$ N/m, and $C_{44} = 22.86$ N/m, which also listed in Table 2. The elastic constants of HSH-C_{10} satisfy the criteria to be a mechanically stable material. Based on the linear elastic constant, Young's modulus (Y) can be calculated using the equation $Y = ({C_{11}}^2\text{-}{C_{12}}^2)/C_{11}$. By multiplying Y and the length of non-periodic direction of the calculation model, the in-plane stiffness (Ys) of HSH-C_{10} is 20 N/m. It is in the same weight with that of germanene (43 N/m) and silicene (62 N/m) computed at the same theoretical level, which have been reported in our previous study [70]. From the above discussion, it could be concluded that HSH-C_{10} also exhibits good mechanical property.

Table 2
Independent elastic constants (C_{ij}, kbar) and in-plane stiffness (Ys, N/m) of HSH-C_{10}, germanene and silicene.

Structure	C_{11}	C_{22}	C_{12}	C_{44}	Ys
HSH-C_{10}	394.14	394.14	348.42	22.86	20
Germanene	318.97	318.97	101.89	108.54	43
Silicene	447.10	447.10	137.43	154.83	62

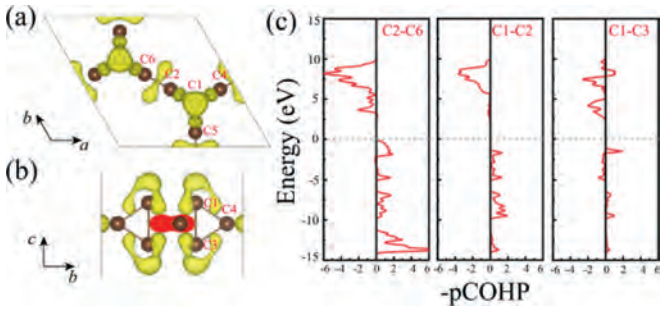

Fig. 3. (a) The top and (b) side views for electron localization function isosurface of HSH-C_{10} with an isovalue of 0.85, and (c) projected crystal orbital Hamilton population (pCOHP) analysis for the bonds of C2-C6, C1-C2, C1-C3. The Fermi level is set at 0 eV.

To get a clear insight of the structural feature displayed in HSH-C_{10}, the chemical bonding is analyzed by the electron localization function (ELF) and projected crystal orbital Hamilton population (pCOHP) [71,72]. ELF can be illustrated as a contour picture in real space with values ranging from 0 to 1. The region 0 means a low electron density area, while 1 indicates the perfect localization of electrons. It plays an important role in understanding the special characteristics of the chemical bonding. The typical kind of bonding in HSH-C_{10} can be seen from ELF isosurface as shown in Figs. 3a and b. Clearly, the isosurface of ELF at 0.85 mainly comprises three localization areas. The first is located in the middle of the $C_{Honeycomb}$-$C_{Honeycomb}$ (C2-C6) within the 2D plane, the second is located in the middle of the $C_{Honeycomb}$-C_{Star} (C1-C2), and the third is located around the C_{Star} atoms (C1, C3). The C2-C6 bond length is 1.30 Å, considerably shorter than the C1-C2 bond with 1.51 Å. Correspondingly, the ELF distribution around the middle of C2-C6 is higher than that of C1-C2, indicating a stronger covalent bonding. Interestingly, there is no evident electron localization between C_{Star}-C_{Star} (C1-C3). The charge is depleted from the center of

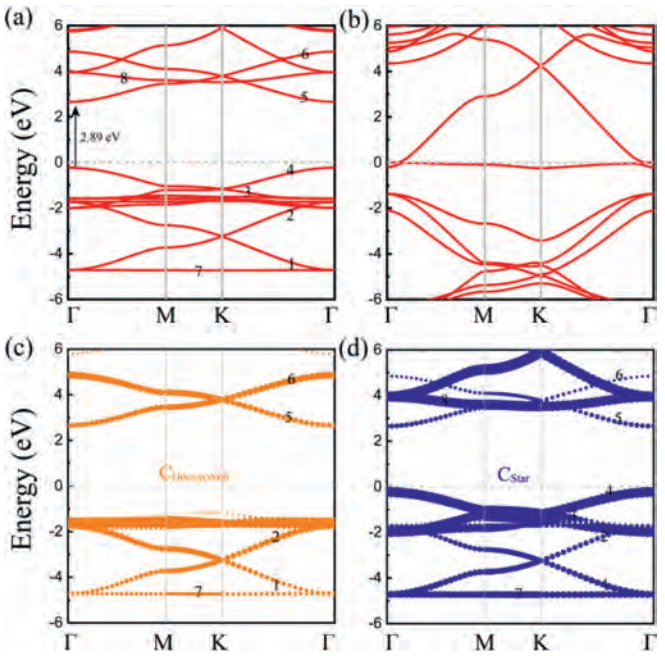

Fig. 4. The band structures for (a) HSH-C_{10} and (b) star carbon monolayer, and (c, d) atom-decomposed band structures along high symmetry direction of the Brillouin zone for HSH-C_{10}. The circle sizes indicate the contribution of atoms in honeycomb or star lattice to the band structure. The Fermi level is set at 0 eV.

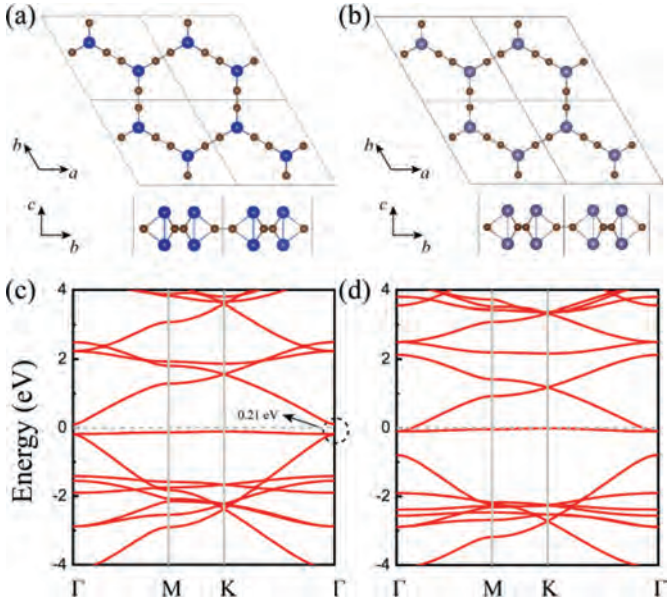

Fig. 5. The top and side views of (a) HSH-C_6Si_4 and (b) HSH-C_6Ge_4, as well as (c, d) the band structures along high symmetry direction of the Brillouin zone. The Fermi level is set at 0 eV.

the hexahedral cage and delocalized onto the bridge carbon atoms, which is a typical feature of charge-shift bond [57–61,73]. Comparing with [1.1.1]propellane, the little longer $C_{Honeycomb}$-$C_{Honeycomb}$ (C1-C3) bond length of 1.67 Å could be attributed to the change in the hybridization of the orbitals of the bridgehead carbon atoms [73]. Importantly, the charge-shift bond leads to the trend that more electrons are distributed outside the *quasi*-2D structure, thus suggesting the potential for applications in molecule adsorption and as a catalyst [74,75].

To well display pCOHPs, the usual way is used by drawing negative contributions to the right and positive to the left, so bonding interaction goes to the right and antibonding interaction goes to the left. From pCOHPs shown in Fig. 3c, it is noticed that the C2-C6 and C1-C2 bonds only fill bonding levels, while the inverted C1-C3 bond exhibits antibonding levels. This is well agreed with the previous observation in the literature that the charge-shift bond exhibits anti-bonding character [57,73]. As a comparison, the pCOHP curves of [1.1.1]propellane is also shown in Fig. S3 (Supporting information), which exhibits the bonding features similar to HSH-C_{10}. Previous studies have reported that the structure could be well stabilized by partial population of the C1-C3 σ-antibonding/bridge π-bonding orbitals [57,58]. Combining the ELF to analyze, the C2-C6 and C1-C2 bonds are the classical covalent bond, while the inverted C1-C3 bond is the charge-shift bond. With ELF and pCOHP curves, the chemical bonding nature of HSH-C_{10} is well captured. As the charge-shift bonding in previous reports normally happens in unique molecules, HSH-C_{10} may open the door to the study of charge-shift bonding in the field of 2D materials.

The structures with a mixed lattice may combine the desirable characteristics of both the honeycomb and star lattices. From electronic band structures shown in Fig. 4a, the PBE results indicate HSH-C_{10} structure is a semiconductor with a direct band gap of 2.89 eV. It is noted that the PBE band gap for T-carbon is 2.25 eV, while it is 4.16 eV for diamond [53]. The honeycomb lattice could induce Dirac bands with the Dirac cone just appear at the Fermi level [4,76], while the star lattice could induce both Dirac bands and flat bands near the Fermi level [3,32], as shown in Fig. 4b. Comparing graphene with Dirac cone at the Fermi level, the band gap of HSH-C_{10} is opened up by the coupling between $C_{Honeycomb}$ and C_{Star} atoms, whereas the two groups of Dirac-like bands separately located on the two sides of Fermi level. To obtain the correlation between the lattice and electronic structure, the atom-decomposed band structures (Figs. 4c and d) along high symmetry direction of the Brillouin zone for HSH-C_{10} are calculated, and the contributions of honeycomb and star lattices thus could be clearly observed. The valence band maximum (VBM) is mainly contributed from carbon atoms in star lattice while the conduction band minimum (CBM) is contributed from atoms in both star and honeycomb lattices. Three groups of Dirac-like bands and two flat bands are numbered from 1 to 8. The Dirac-like bands which numbered as 3, 4 and flat bands numbered as 8 are contributed from the carbon atoms in star lattice, while the Dirac-like bands numbered as 1, 2, 5, 6 and flat band numbered as 7 are contributed from the atoms in honeycomb lattice and star lattice. From the above discussion, the coupling of honeycomb and star lattices leads to the result that HSH-C_{10} loses the metallic character in graphene and carbon allotrope with star lattice, but it retains some characteristics like flat band and Dirac bands.

The electronic band structure is affected by the strength of coupling between atoms in honeycomb and star lattice, so it could be modulated by substituting atoms in the HSH lattice. Since silicon and germanium atoms have larger covalent radius and higher energy levels than carbon atoms, they are used to replace carbon atoms in honeycomb lattice, and the new structures are named as HSH-C_6Si_4 and HSH-C_6Ge_4. The optimized crystal structures with top and side views are shown in Figs. 5a and b, and the equilibrium lattice constants are estimated to be 7.55 and 7.81 Å. The bond lengths of C-Si and C-Ge are 1.94 and 2.08 Å, respectively. Phonon dispersion indicates that the structures are dynamically stable, as shown in Figs. S4a and b (Supporting information). The band structures would be acquired by including the couplings between the silicon (or germanium) atoms in honeycomb lattice and carbon atoms in star lattice. Different from HSH-C_{10} with a large band gap, the HSH-C_6Si_4 system exhibits semiconductor with a band gap of 0.21 eV, while HSH-C_6Ge_4 is metallic. This is be-

cause the coupling between the carbon and silicon (or germanium) atoms is weaker than the $C_{Honeycomb}$-C_{Star} coupling in HSH-C_{10}. As illustrated in Figs. 5c and d, a flat band occurs near the Fermi energy for HSH-C_6Si_4 and HSH-C_6Ge_4. Interestingly, the flat band is attached to the upper Dirac-like band for HSH-C_6Si_4, while it is attached to the lower one for HSH-C_6Ge_4. The unique electronic structure renders HSH-C_6Si_4 and HSH-C_6Ge_4 potential 2D materials for application in nanoelectronics. The coexistence of flat and steep bands near the Fermi level is regarded as an important condition for the superconductivity of materials [77,78]. All the results indicate that HSH lattice could combine the electronic characteristics of both the honeycomb and star lattices and expand the diversity of 2D materials.

In summary, we designed a new HSH lattice and reported a new *quasi*-2D carbon allotrope named HSH-C_{10}. Total energy, phonon dispersion, molecular dynamic simulations, as well as elastic constants calculations indicate the structure has good stability. Through chemical bonding analysis by ELF and pCOHP, the C2-C6 and C1-C2 bonds of HSH-C_{10} are classical covalent bonds, while the inverted C1-C3 bond is described as a charge-shift bond, which is strong and shows large covalent-ionic resonance interaction energy. What is more, the charge-shift bond leads to the trend that more electrons are distributed outside the 2D plane of HSH-C_{10}, suggesting a potential for applications in molecule adsorption and as a catalyst. It is expected that the HSH-C_{10} could be synthesized by the polymerization of [1.1.1]propellane, and would be a fascinating 2D carbon allotrope for its unique structure and intriguing reactivity. As the first reported 2D material with charge-shift bond, HSH-C_{10} may open the door for understanding charge-shift bonding in fundamental chemistry and physics, as well as other fields in application. The results of the calculated electronic band structures show that HSH-C_{10} carbon is a semiconductor with a direct band gap of 2.89 eV and could combine the desirable characteristics of honeycomb and star lattice. To modulate the electronic band structure to the potential application in nanoelectronics, by replacing carbon element in honeycomb lattice with silicon and germanium, new structures named HSH-C_6Si_4 and HSH-C_6Ge_4 are also obtained. Different from HSH-C_{10} with a large band gap, the HSH-C_6Si_4 system exhibits semiconductor with a band gap of 0.21 eV, while HSH-C_6Ge_4 is metallic. With different elements in the sub-lattice, combination of the desirable characteristics of both the honeycomb and star lattices could be realized, and the physical and chemical properties would be modulated. All the results indicate that HSH lattice would be used to derive the charge-shift bond family, increase the structural diversity of 2D materials and has potential in probing or engineering chemical and physical properties. This study may provide a creative platform to study the exotic properties of HSH lattice and stimulate more efforts on the research field of mixed lattice.

Declaration of competing interest

The authors declare that they have no known competing financial interests or personal relationships that could have appeared to influence the work reported in this paper.

Acknowledgments

This work is partially supported by the National Natural Science Foundation of China (Nos. 21773124, 12134019), by the Fundamental Research Funds for the Central Universities (Nankai University, No. 63213042), by the Ph.D. Candidate Research Innovation Fund of Nankai University, Science and Technology Research Project of Hubei Provincial Department of Education (No. D20212603) and Hubei University of Arts and Science (Nos. 2020kypytd001, 2020kypytd002, XK2021024). This work is also supported by the Supercomputing Center of Nankai University (NKSC).

Supplementary materials

Supplementary material associated with this article can be found, in the online version, at doi:10.1016/j.cclet.2021.11.027.

References

[1] C.L. Kane, E.J. Mele, Phys. Rev. Lett. 95 (2005) 146802.
[2] H.M. Guo, M. Franz, Phys. Rev. B 80 (2009) 113102.
[3] M. Chen, S. Wan, J. Phys. Condens. Matter 24 (2012) 325502.
[4] C. Barreteau, F. Ducastelle, T. Mallah, J. Phys. Condens. Matter 29 (2017) 465302.
[5] L. Du, X. Zhou, G.A. Fiete, Phys. Rev. B 95 (2017) 035136.
[6] Z.F. Wang, K.H. Jin, F. Liu, WIREs. Comput. Mol. Sci. 7 (2017) e1304.
[7] Z. Liu, F. Liu, Y.S. Wu, Chin. Phys. B 23 (2014) 12.
[8] D. Leykam, A. Andreanov, S. Flach, Adv. Phys. X 3 (2018) 1473052.
[9] J. Yu, C. He, C. Pu, et al., Chin. Chem. Lett. 32 (2021) 3149–3154.
[10] S. Yuan, B. Xu, S. Li, et al., Chin. Chem. Lett. 33 (2022) 399–403.
[11] S. Zhao, J.L. Zhang, W. Chen, Z. Li, J. Phys. Chem. C. 124 (2020) 2024–2029.
[12] L. Zhao, Y. Li, G. Zhou, et al., Chin. Chem. Lett. 32 (2021) 900–905.
[13] M. Qiao, Y. Wang, Y. Li, Z. Chen, J. Phys. Chem. C 121 (2017) 9627–9633.
[14] S. Li, M. Shi, J. Yu, et al., Chin. Chem. Lett. 32 (2021) 1977–1982.
[15] R. Xu, X. Zou, B. Liu, H.M. Cheng, Mater. Today 21 (2018) 391–418.
[16] J. Wang, S. Deng, Z. Liu, Z. Liu, Natl. Sci. Rev. 2 (2015) 22–39.
[17] L. Ye, M. Kang, J. Liu, et al., Nature 555 (2018) 638.
[18] X. Li, Y. Dai, Y. Ma, et al., Carbon 109 (2016) 788–794.
[19] M. Maruyama, N.T. Cuong, S. Okada, Carbon 109 (2016) 755–763.
[20] C. Zhong, Y. Xie, Y. Chen, S. Zhang, Carbon 99 (2016) 65–70.
[21] W. Tong, Q. Wei, H.Y. Yan, M.G. Zhang, X.M. Zhu, Front. Phys. 15 (2020) 63501.
[22] R.S. Zhang, J.W. Jiang, Front. Phys. 14 (2018) 13401.
[23] A.K. Geim, K.S. Novoselov, Nat. Mater. 6 (2007) 183–191.
[24] M. Houssa, A. Dimoulas, A. Molle, J. Phys. Condens. Matter 27 (2015) 253002.
[25] B. Mortazavi, O. Rahaman, M. Makaremi, et al., Phys. E Low-dimens. Syst. Nanostruct. 87 (2017) 228–232.
[26] S. Balendhran, S. Walia, H. Nili, S. Sriram, M. Bhaskaran, Small 11 (2015) 640–652.
[27] S. Thomas, H. Li, C. Zhong, et al., Chem. Mater. 31 (2019) 3051–3065.
[28] Y. Jing, T. Heine, J. Am. Chem. Soc. 141 (2019) 743–747.
[29] E. Liu, Y. Sun, N. Kumar, et al., Nat. Phys. 14 (2018) 1125–1131.
[30] S. Huang, Y. Xie, C. Zhong, Y. Chen, J. Phys. Chem. Lett. 9 (2018) 2751–2756.
[31] Z. Li, J. Zhuang, L. Wang, et al., Sci. Adv. 4 (2018) eaau4511.
[32] X.L. Fan, C.Y. Niu, X.Q. Wang, J.T. Wang, H.D. Li, Chin. Phys. B 23 (2014) 096104.
[33] T. Morresi, A. Pedrielli, S.A. Beccara, et al., Carbon 159 (2020) 512–526.
[34] T. Mizoguchi, M. Maruyama, S. Okada, Y. Hatsugai, Phys. Rev. Mater. 3 (2019) 114201.
[35] J.L. Lu, W. Luo, X.Y. Li, et al., Chin. Phys. Lett. 34 (2017) 057302.
[36] H. Pan, Y. Han, J. Li, et al., Phys. Chem. Chem. Phys. 20 (2018) 14166–14173.
[37] H. Li, Y. Xu, X. Sun, S. Wang, J. Alloy. Compd. 765 (2018) 969–976.
[38] L. Song, L. Zhang, Y. Guan, et al., Mater. Res. Express 6 (2019) 075911.
[39] L. Zhang, C.W. Zhang, S.F. Zhang, et al., Nanoscale 11 (2019) 5666–5673.
[40] T.T. Song, M. Yang, J.W. Chai, et al., Sci. Rep. 6 (2016) 29221.
[41] V.O. Garlea, L.D. Sanjeewa, M.A. McGuire, et al., Phys. Rev. X 9 (2019) 011038.
[42] G. Kresse, J. Furthmüller, Comput. Mater. Sci. 6 (1996) 15–50.
[43] G. Kresse, J. Furthmüller, Phys. Rev. B 54 (1996) 11169–11186.
[44] J.P. Perdew, K. Burke, M. Ernzerhof, Phys. Rev. Lett. 77 (1996) 3865–3868.
[45] P.E. Blöchl, Phys. Rev. B 50 (1994) 17953–17979.
[46] A. Togo, I. Tanaka, Scr. Mater. 108 (2015) 1–5.
[47] S. Baroni, S. de Gironcoli, A. Dal Corso, P. Giannozzi, Rev. Mod. Phys. 73 (2001) 515–562.
[48] K.S. Novoselov, A.K. Geim, S.V. Morozov, et al., Science 306 (2004) 666.
[49] D. Sen, B.K. Das, S. Saha, et al., Carbon 146 (2019) 430–437.
[50] L.C. Xu, R.Z. Wang, M.-.S. Miao, et al., Nanoscale 6 (2014) 1113–1118.
[51] Z. Jia, Y. Li, Z. Zuo, et al., Acc. Chem. Res. 50 (2017) 2470–2478.
[52] L. Li, X. Kong, F.M. Peeters, Carbon 141 (2019) 712–718.
[53] X.L. Sheng, Q.B. Yan, F. Ye, Q.R. Zheng, G. Su, Phys. Rev. Lett. 106 (2011) 155703.
[54] J. Zhang, R. Wang, X. Zhu, et al., Nat. Commun 8 (2017) 683.
[55] K.B. Wiberg, F.H. Walker, J. Am. Chem. Soc. 104 (1982) 5239–5240.
[56] R. Gianatassio, J.M. Lopchuk, J. Wang, et al., Science 351 (2016) 241.
[57] A.J. Sterling, A.B. Dürr, R.C. Smith, E.A. Anderson, F. Duarte, Chem. Sci. 11 (2020) 4895–4903.
[58] S. Shaik, D. Danovich, W. Wu, P.C. Hiberty, Nat. Chem. 1 (2009) 443–449.
[59] S. Shaik, D. Danovich, J.M. Galbraith, et al., Angew. Chem. Int. Ed. 59 (2020) 984–1001.
[60] S. Shaik, Z. Chen, W. Wu, et al., ChemPhysChem 10 (2009) 2658–2669.
[61] W. Wu, J. Gu, J. Song, S. Shaik, P.C. Hiberty, Angew. Chem. Int. Ed. 48 (2009) 1407–1410.
[62] E. Honegger, H. Huber, E. Heilbronner, W.P. Dailey, K.B. Wiberg, J. Am. Chem. Soc. 107 (1985) 7172–7174.
[63] W. Yu, C.Y. Niu, Z. Zhu, X. Wang, W.B. Zhang, J. Mater. Chem. C 4 (2016) 6581–6587.
[64] M. Naseri, S. Lin, J. Jalilian, J. Gu, Z. Chen, Front. Phys. 13 (2018) 138102.

[65] D. Liu, A.G. Every, D. Tománek, Phys. Rev. B 94 (2016) 165432.
[66] Q. Gao, X. Zhuang, S. Hu, Z. Hu, J. Phys. Chem. C 124 (2020) 4644–4651.
[67] L. Wirtz, A. Rubio, Solid State Commun 131 (2004) 141–152.
[68] S. Zhang, J. Zhou, Q. Wang, et al., Proc. Natl. Acad. Sci. 112 (2015) 2372.
[69] Y. Ding, Y. Wang, J. Phys. Chem. C 117 (2013) 18266–18278.
[70] L. Zhang, J. Pan, Q. Yan, Z. Hu, Phys. Status. Solidi. RRL 14 (2020) 2000324.
[71] V.L. Deringer, A.L. Tchougréeff, R. Dronskowski, J. Phys. Chem. A 115 (2011) 5461–5466.
[72] S. Maintz, V.L. Deringer, A.L. Tchougréeff, R. Dronskowski, J. Comput. Chem. 37 (2016) 1030–1035.
[73] J. Joy, E. Akhil, E.D. Jemmis, Phys. Chem. Chem. Phys. 20 (2018) 25792–25798.
[74] S. Tang, Q. Dang, T. Liu, et al., J. Am. Chem. Soc. 142 (2020) 19308–19315.
[75] M.R. Ashwin Kishore, A.O. Sjåstad, P. Ravindran, Carbon 141 (2019) 50–58.
[76] M. Gmitra, S. Konschuh, C. Ertler, C. Ambrosch-Draxl, J. Fabian, Phys. Rev. B 80 (2009) 235431.
[77] S. Deng, A. Simon, J. Köhler, Angew. Chem. Int. Ed. 37 (1998) 640–643.
[78] C.X. Zhao, Y.Q. Yang, C.Y. Niu, J.Q. Wang, Y. Jia, Comput. Mater. Sci. 160 (2019) 115–119.